

In Situ Synthesis and Electrochemical Properties of Fe/Li₂O as a High-Capacity Cathode Prelithiation Additive for Lithium Ion Batteries

Jusheng Zheng, Kui Liang*, Kaiyue Shi, Yechao Qiu

College of Materials Science and Engineering, Hunan University, Changsha, 410082, China

*E-mail: liangkui363@163.com

Received: 6 February 2019 / Accepted: 11 March 2019 / Published: 10 May 2019

The irreversible capacity loss in the first cycle significantly reduces the specific capacity of lithium ion batteries. Cathode prelithiation is a common method to alleviate this problem. Here, Fe/Li₂O were successfully prepared by *in situ* solid phase reaction method. Fe/Li₂O as a cathode prelithiation additive has a high prelithiation specific capacity of 447.3 mAh g⁻¹ during charging, and the first charge capacity of LiNi_{0.6}Co_{0.2}Mn_{0.2}O₂ with 7.5% Fe/Li₂O additive could be enhanced by 9.1% and its cycling stability was improved from 86.9% to 90.2% after 70 cycles. The cathode prelithiation additive remarkably enhanced the content of active lithium during the initial delithiation process, contributing the formation of solid electrolyte interphase on the anode surface and better cycling stability. This easy-operating cathode prelithiation method could obtain evident effect of prelithiation and had good compatibility with existing lithium ion batteries.

Keywords: Irreversible capacity loss; Fe/Li₂O; *In situ* synthesis; Cathode prelithiation additive; Lithium ion battery

1. INTRODUCTION

At present, lithium ion batteries are widely used in a variety of hybrid electric vehicles, grid-scale energy storage and portable electronic devices [1-5]. Commercial lithium ion batteries usually consist of two electrodes: a layered lithium transition metal oxide cathode (such as LiCoO₂ and LiNi_{0.6}Co_{0.2}Mn_{0.2}O₂) and a graphite anode. The irreversible capacity loss of lithium ion batteries during the first charge and discharge is mainly due to the formation of solid electrolyte interphase (SEI) at the anode surface, which consumes approximately 10-20% of active lithium from the cathode, resulting in low first cycle coulombic efficiency and cycling stability and lower energy density [6-10]. A prelithiation additive can significantly enhance the content of active lithium to compensate the loss of lithium during the first cycle. Therefore, the prelithiation additives which were classified as anode and cathode

prelithiation additives have gained great attention and been extensively investigated in recent decades. Anode prelithiation additives commonly include stabilized lithium metal powder and lithium silicide [11–16,23], and cathode prelithiation additives mainly include lithium-rich compounds and lithium-containing composites, such as Li_3N [17,18], Li_6CoO_4 [19], Li_5FeO_4 [20–23], Metal/LiF [24] and Metal/ Li_2O [25].

According to previous studies on cathode prelithiation additives, they generally possess the following characteristics. Firstly, cathode prelithiation additives have a high theoretical prelithiation capacity reaching 400 mAh g^{-1} or more. Secondly, the prelithiation additives release most of active lithium ions below the maximum potential during cathode charging, but active lithium ions almost cannot be embedded back into the cathode under the minimum potential during cathode discharging. Thirdly, such prelithiation additives have prominent compatibility with the active materials, common solvents and suitable binders during the preparation processes of the existing lithium ion batteries [25]. Wenquan Lu et al. claimed that the $\text{LiNi}_{0.5}\text{Co}_{0.2}\text{Mn}_{0.3}\text{O}_2/\text{SiO}$ full cell with 9.1% Li_5FeO_4 additive was 22% higher reversible capacity than that of the pristine $\text{LiNi}_{0.5}\text{Co}_{0.2}\text{Mn}_{0.3}\text{O}_2$ electrode and its cycling performance was improved from 90.94% to 98.92% after 50 cycles [23]. Yi Cui et al. reported that the reversible capacity of the $\text{LiFePO}_4/\text{graphite}$ full cell with 4.8% $\text{Co}/\text{Li}_2\text{O}$ additive could be improved by 11% [25]. They claimed that the compensation effect of the active lithium is obvious, but several disadvantages exist for preparing these cathode prelithiation additives, such as the high cost of raw materials, the harshness of preparation condition and the longer sintering time.

There have been many reports about lithium-containing composites being used as cathode prelithiation additives, such as Metal/ Li_2O , Metal/LiF. The transition metal or Li_2O particles in Metal/ Li_2O composites must be guaranteed to be nanoscales, in order to have a prelithiated effect on electrodes. This means that the preparation of the desirable Metal/ Li_2O particles is quite crucial. However, according to previous studies, it is difficult to prepare the desirable lithium-containing composites because residual reactants and intermediate phases may exist in the composite particles prepared by conversion reaction of transition metal oxides with lithium metal [24,25].

Here, $\text{Fe}/\text{Li}_2\text{O}$ were successfully prepared by *in situ* solid phase reaction method. The accessible raw materials and the controllable preparation conditions contribute to the formation of desirable composite particles and sufficiently exhibit the superiority of our method. We find that the $\text{Fe}/\text{Li}_2\text{O}$ are used as cathode prelithiation additive which have excellent compatibility with the active materials, common solvents and suitable binders during the preparation processes of the existing lithium ion batteries, and the addition of the additive to $\text{LiNi}_{0.6}\text{Co}_{0.2}\text{Mn}_{0.2}\text{O}_2$ electrode has a good prelithiated effect. In addition, the use of this additive is not accompanied by the evolution of undesired gas in the initial deintercalation process, thus will not bring about potential safety hazard.

2. EXPERIMENTAL SECTION

2.1 Preparation of $\text{Li}_2\text{CO}_3/\text{C}$ composites as precursor

Li_2CO_3 (Aladdin Biochemical Technology Co., Ltd., Shanghai, China) was mixed with carbon black (Hexing Chemical Industry Co., Ltd., Jiaozuo, China) in the mass ratio of 3.7:1.3, and the

generated mixture was loaded into 100 ml Teflon vessel containing an appropriate amount of deionized water to form the solid-liquid mixture which was then sonicated for 20 min for the purpose of forming the suspension solution, and the suspension solution was heated at 160 °C for 6 h to obtain the $\text{Li}_2\text{CO}_3/\text{C}$ composites.

2.2 Preparation of Fe/Li₂O by *in situ* calcination

Fe/Li₂O were prepared by *in situ* solid phase reaction in the vacuum tube furnace. The prepared $\text{Li}_2\text{CO}_3/\text{C}$ composites and $\text{FeC}_2\text{O}_4 \cdot 2\text{H}_2\text{O}$ (Aladdin Biochemical Technology Co., Ltd., Shanghai, China) were further mixed according to the molar ratio of lithium to iron of 3:1 and sufficiently ground. The ground mixture was then compacted and placed in the ceramics tube, and the ceramics tube was evacuated to a vacuum of about 19 Pa and heated at 850 °C for 3.5 h to obtain the Fe/Li₂O.

2.3 Electrode preparation

The preparation of the $\text{LiNi}_{0.6}\text{Co}_{0.2}\text{Mn}_{0.2}\text{O}_2$ (NCM622, Changyuan Lico Co., Ltd., Hunan, China)-Fe/Li₂O cathode was implemented in an argon-filled glove box in the light of following procedures. Fe/Li₂O firstly blended with NCM622 at a weight ratio of 3:37 for 20 min to form NCM622-Fe/Li₂O which then mixed with Acetylene black and polyvinylidene fluoride (PVDF) binder in the weight ratio of NCM622-Fe/Li₂O: acetylene black: PVDF=8:1:1 in an appropriate amount of N-methylpyrrolidone (NMP) to form a homogenous slurry. The slurry was coated on a pre-cleaned aluminum foil, and dried in a vacuum oven at 80 °C for 12 h. The cathode electrodes were stored in an argon-filled glove box before assembled into coin cells. Pristine Fe/Li₂O and pristine NCM622 cathode electrodes were prepared by the same preparation procedures as above.

2.4 Characterization

The composition and crystal structure of the Fe/Li₂O sample was identified by Powder X-ray diffraction (XRD; D8 Discover 2500, Bruker Co., Germany) with a Cu-K α radiation. Field emission scanning electron microscopy (FE-SEM; SU8820, Hitachi Co., Japan) and transmission electron microscope (TEM; FEI Tecnai G2 F20 S-TWIX) were used to observe the morphologies of the Fe/Li₂O and NCM622-Fe/Li₂O samples. X-ray photoelectron spectroscopy (XPS; K-Alpha 1063, Thermo Fisher Scientific, United Kingdom) was performed to investigate the bonding characterization of the products converting from the pristine Fe/Li₂O at the different cut-off voltage states during initial charging process.

2.5 Electrochemical measurement

The electrochemical test of the NCM622-Fe/Li₂O, pristine Fe/Li₂O and pristine NCM622 samples in CR2032 coin-type cells were carried out, respectively. A complete coin-type cell consists of a cathode electrode and a counter electrode separated by a polyethylene film (Celgard 2400) with

electrolyte. NCM622-Fe/Li₂O, pristine Fe/Li₂O and pristine NCM622 were used as the cathode electrodes, respectively. Lithium metal was used as the anode electrode, and the electrolyte was 1M LiPF₆ dissolved in ethylene carbonate (EC), dimethyl carbonate (DMC) and ethylene methyl carbonate (EMC) at a volume ratio of 1:1:1. All coin-type cells were assembled in an argon-filled glove box. Cycling stability and the reversible capacity characteristics were carried out on a battery testing system (Neware CT3008, China) by recording the constant current charge-discharge curves in the voltage range of 2.7-4.3 V. The pristine Fe/Li₂O was performed under a small current of 1/400 C for 10 h at the initial phase of the first charging process in order to prevent a rapid increase of potential, and then continued to be charged and discharged between 2.7 and 4.3 V at 1/40 C (1C=798 mAh g⁻¹) at room temperature for the sake of obtaining their first cycling curve. The electrochemical charge-discharge curves of the NCM622-Fe/Li₂O and pristine NCM622 were firstly tested at a current density of 1/20 C (1C=170 mAh g⁻¹) for two cycles, and then the cycling stabilities were implemented at a current density of 1/5 C for 70 cycles. The cyclic voltammetry (CV) was tested on electrochemical workstation (CHI604E, China) and its curve was collected in the voltage range of 3.0-4.5 V (vs. Li/Li⁺) at a scan rate of 0.1 mV s⁻¹.

3. RESULTS AND DISCUSSION

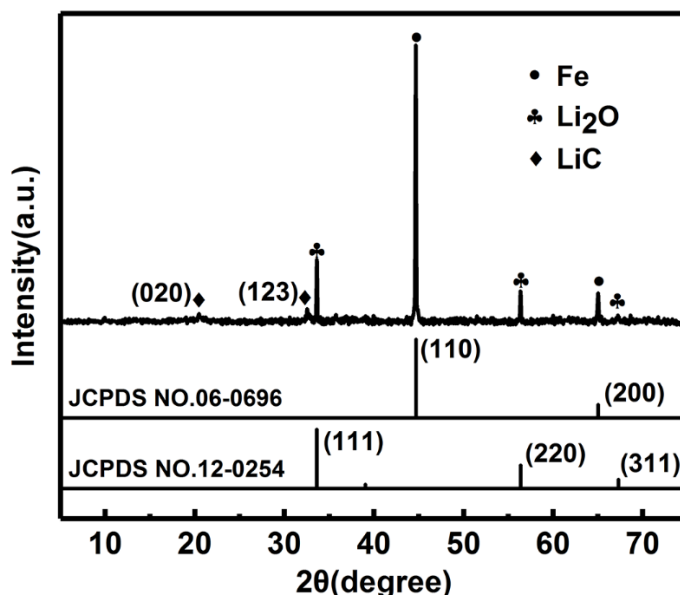
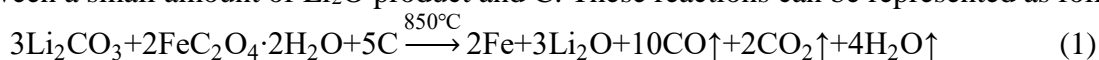


Figure 1. XRD pattern of the Fe/Li₂O sample.

Fig. 1 shows that the X-ray diffraction (XRD) pattern of the Fe/Li₂O sample. Diffraction peaks can be well indexed to Fe (JCPDS No.06-0696) with body-centered-cubic (*Im-3m*) and Li₂O (JCPDS No.12-0254) with face-centered cubic structure (*Fm-3m*). It indicates that FeC₂O₄·2H₂O and Li₂CO₃ were converted into Fe and Li₂O by the carbothermic reduction method. The sharp diffraction peaks of Fe and Li₂O indicate the good crystallinity of the prepared composite particles. In addition, a very small

amount of LiC impurity (JCPDS No.14-0649) can be detected in the Fe/Li₂O sample due to the side reaction between a small amount of Li₂O product and C. These reactions can be represented as follows:



SEM images of the Fe/Li₂O and NCM622-Fe/Li₂O samples are shown in Fig. 2. Fig. 2(a and b) show that the Fe/Li₂O powder is composed of the micro-sized secondary particles agglomerated from the primary Fe/Li₂O particles, and primary Fe/Li₂O particles with spherical characteristics can contribute to improving mutual contact of the composite particles. In Fig. 2(c and d), the NCM622-Fe/Li₂O sample composed of the spheroidal NCM622 particles and micro-sized secondary Fe/Li₂O particles which are filled in the interstices among the spheroidal NCM622 particles.

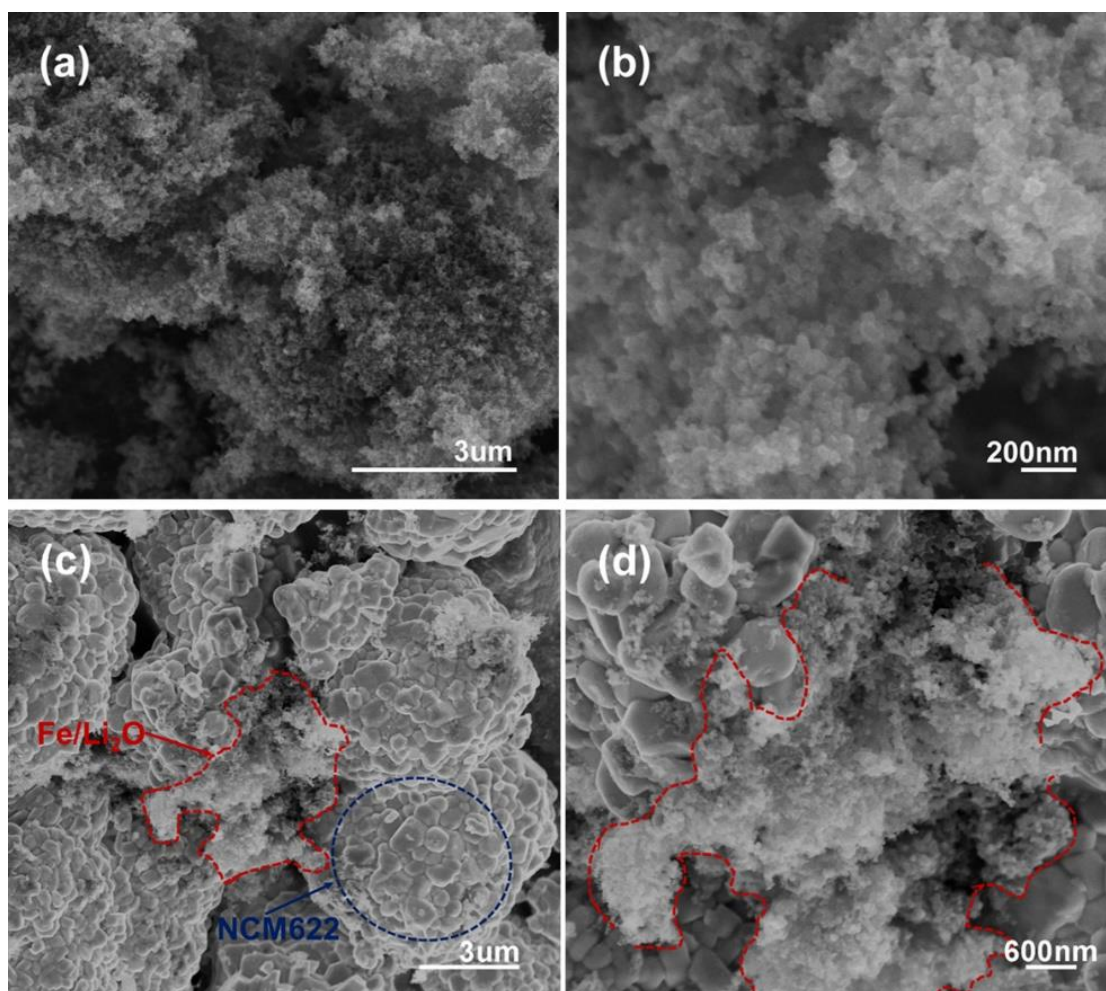


Figure 2. SEM images of the specimens: (a), (b) Fe/Li₂O; (c), (d) NCM622-Fe/Li₂O.

To better observe the microstructure of the primary Fe/Li₂O particles, TEM images of the Fe/Li₂O sample are shown in Fig. 3. Numerous spheroidal nanosized Fe/Li₂O particles with the size of ~100 nm is observed (Fig. 3(a)). As shown in Fig. 3(b), the structures of the metallic iron and Li₂O

nanoclusters dispersed in the carbon matrix. The nanocrystal regions with the darkest contrast can be related to metallic iron, while the nanoclusters with slight bright background can be referred to Li_2O in the carbon matrix, because the former (Fe) is more visible than lower atomic number element (Li) which has weak scattering of light constituent element in the bright field image during TEM image formation [26,27]. HRTEM images analysis of the dark nanoregions in the Fe/ Li_2O sample are shown in Fig. 3(c and d). Lattice fringes with spacings of 0.2 and 0.27 nm of the nanoparticle can be clearly observed (Fig. 3(d)), corresponding to the (110) crystal planes of metallic iron and the (111) crystal planes of Li_2O , respectively. The results indicate that *in situ* formed Fe and Li_2O nanoparticles are dispersed in the composites, in consistent with the XRD result (Fig. 1). The nanosized Fe/ Li_2O composites ensure intimate contact between the metallic iron and Li_2O nanoparticles, hence significantly shorten the diffusion path for both of lithium ions and electrons when such composites are used as the cathode material for lithium ion batteries [27].

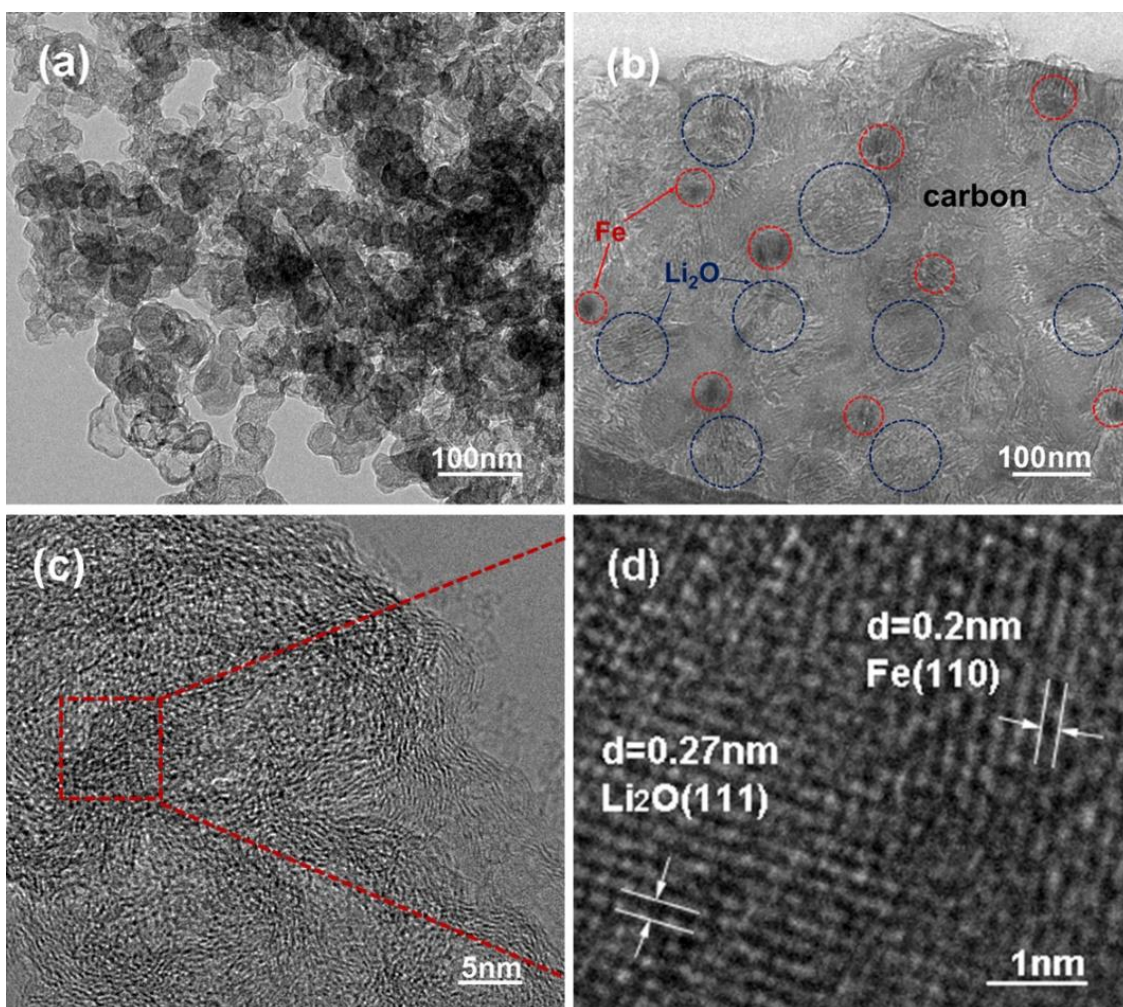


Figure 3. (a), (b) the TEM images of the Fe/ Li_2O sample; (c), (d) HRTEM images of the dark nanoregions in the Fe/ Li_2O sample.

The first charge-discharge curve of pristine Fe/ Li_2O between 2.7 V and 4.3 V at 1/40 C is shown in Fig. 4(a). The pristine Fe/ Li_2O reveals that the first charge specific capacity is up to 447.3 mAh g^{-1}

and its first discharge specific capacity is only 6.9 mAh g^{-1} . The delithiation process of the Fe/Li₂O is almost completely irreversible during the first discharge, meaning that Fe/Li₂O can be used as a cathode prelithiation additive within this voltage range. Fig. 4(b) displays the first charge-discharge curves of the pristine NCM622 and NCM622-Fe/Li₂O between 2.7 V and 4.3 V at 1/20 C rate, respectively. The NCM622-Fe/Li₂O delivers the first charge capacity of 231.4 mAh g^{-1} , improving by 9.1% compared to that of the pristine NCM622. The improvement of the charge capacity of the NCM622-Fe/Li₂O can be attributed to the capacity released by active lithium from 7.5% Fe/Li₂O additive. The shape of the first charge-discharge curves of the two samples are similar, indicating that a small amount of the Fe/Li₂O can be well compatible with the active materials of NCM622 cathode. A summary of the results of first cycle performances of different samples are provided in Table 1. First discharge capacity of the NCM622-Fe/Li₂O is 173.7 mAh g^{-1} (based on the weight of NCM622 and Fe/Li₂O), and the conversion of NCM622-Fe/Li₂O into the expected NCM622 shows a first discharge capacity of 187.2 mAh g^{-1} and its coulombic efficiency is improved from 85.5% to 87.5% (based on the weight of NCM622 alone). The results indicate that Fe/Li₂O prelithiation additive can contribute to improving the coulombic efficiency of NCM622. Fig. 4(c) exhibits the charge-discharge curves of the NCM622-Fe/Li₂O at 1/20 C rate for the initial three cycles. The NCM622-Fe/Li₂O delivers a first charge capacity of 231.4 mAh g^{-1} and the coulombic efficiency of 75.1% for the initial cycle, indicating a large irreversible capacity loss. The large irreversible capacity loss is mainly attributable to two factors. One is that the transition metal (TM) ions which have similar size to lithium ion in NCM622 active material migrate into vacancies of lithium and prevent active lithium ions from returning to original position, resulting in Li/TM cations mixing during the lithiation process [28-30]. Another is that active lithium ions of Fe/Li₂O prelithiation additive are hardly embedded back into NCM622-Fe/Li₂O cathode during discharging. The discharge capacity slowly increases for the initial three cycles and reaches 176.3 mAh g^{-1} in the third cycle. Due to the Fe/Li₂O additive is able to significantly increase the content of active lithium during the initial delithiation process, conducting to form stable passivated film on the anode surface and achieve stable discharge capacity in these cycles [16,25]. Fig. 4(d) shows the cyclic performance of the NCM622-Fe/Li₂O and NCM622 between 2.7 V and 4.3 V at 1/5 C rate for 70 cycles. The NCM622-Fe/Li₂O delivers a first discharge specific capacity of 153.7 mAh g^{-1} , which is slightly less than that (163.6 mAh g^{-1}) of NCM622, but the ratio of capacity retention is improved from 86.9% to 90.2% after 70 cycles. Because the Fe/Li₂O additive releases almost all active lithium ions to compensate for the lithium loss due to the formation of solid electrolyte interphase on the anode surface during the first charge, thereby acquiring better cycling stability [16,25]. Both of the NCM622 electrodes with and without the Fe/Li₂O additive show high discharge capacity and stable cycling performance, suggesting that the Fe/Li₂O additive almost has not any negative effects on the cycling stability of cathode.

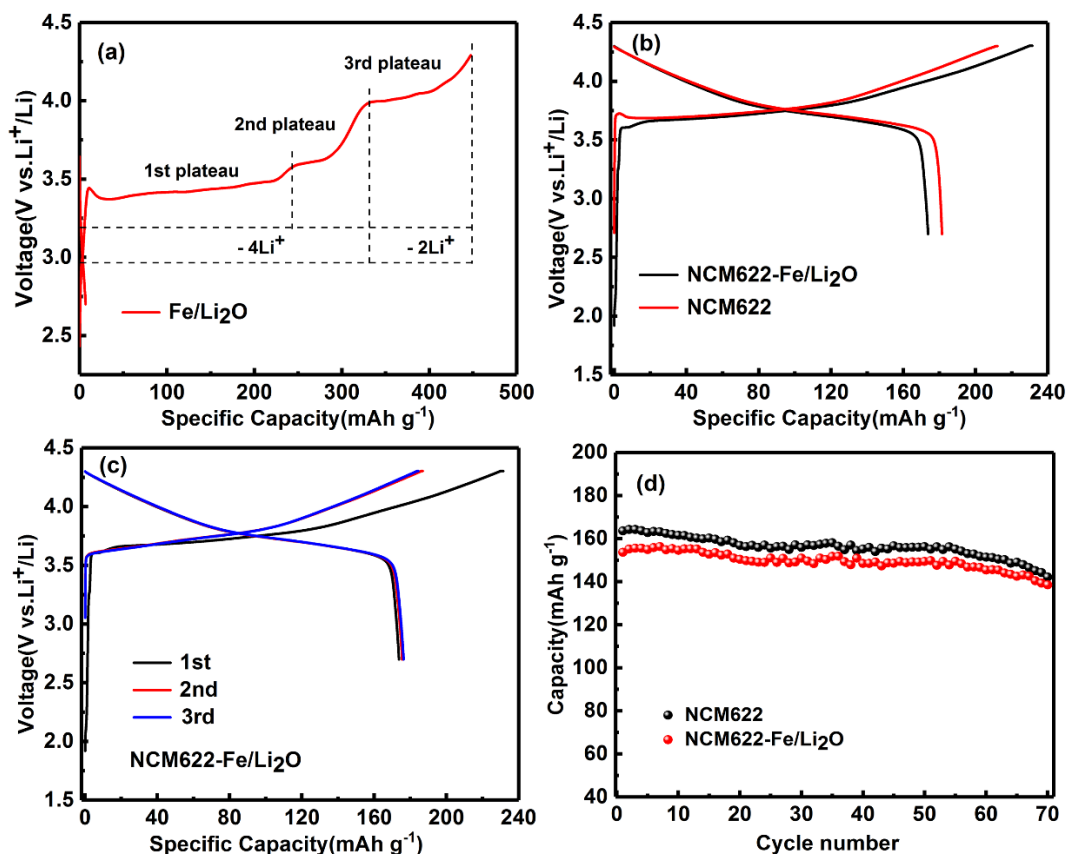


Figure 4. (a), (b) First discharge/charge curve of pristine Fe/Li₂O at 1/40 C (1 C=798 mAh g⁻¹), NCM622-Fe/Li₂O and pristine NCM622 at 1/20 C (1 C=170 mAh g⁻¹). (c) 1st, 2nd and 3rd discharge/charge curves of NCM622-Fe/Li₂O at 1/20 C. (d) cycling performances of NCM622-Fe/Li₂O and pristine NCM622 at 1/5 C.

Table 1. Summary of 1st cycle performances of different samples.

sample	1 st charge (mAh g ⁻¹)	1 st discharge (mAh g ⁻¹)	Coulombic efficiency(%)
pristine NCM622	212.1	181.4	85.5%
pristine Fe/Li ₂ O	447.3	6.9	/
NCM622-Fe/Li ₂ O	231.4	173.7	75.1%
NCM622 expected	213.9	187.2	87.5%

In order to better confirm the conversion products of Fe/Li₂O during the initial delithiation process. Fig. 5 Shows the XPS spectra of the pristine Fe/Li₂O electrode surface under the cut-off voltage states of 3.9 V and 4.3 V during the first constant-current charging. The Fe 2p and O 1s spectra of the electrode surface at charged to 3.9 V state are shown in Fig. 5(a and b). The Fe 2p spectrum (Fig. 5(a)) shows that the binding energies of Fe 2p_{3/2} and Fe 2p_{1/2} peaks are located at 710.9 eV and 724.4 eV, respectively. This is feature of Fe²⁺ and Fe³⁺ in Fe₃O₄ [31-33]. The O 1s spectrum exhibits two peaks (Fig. 5(b)). Peak at 530.6 eV corresponds to crystal lattice oxygen bonded with iron in Fe₃O₄ [31,33,34], and peak at 531.7 eV is owed to adsorbed -OH on the surface of the Fe/Li₂O electrode [34]. The Fe 2p and O 1s spectra of the electrode surface at charged to 4.3 V state are shown in Fig. 5(c and d). Fig. 5(c)

shows that the dominant Fe 2p_{3/2} peak is located at 710.6 eV and the Fe 2p_{1/2} feature is situated in 723.9 eV, corresponding to the Fe³⁺-O bonds [32,35,36]. As shown in Fig. 5(d), O 1s spectrum displays two peaks. Peak at 530.5 eV is well accordance with crystal lattice oxygen bonded with Fe³⁺ in Fe₂O₃ [36], and peak at 531.4 eV is attributed to adsorbed -OH on the surface of the Fe/Li₂O electrode, which is roughly in accordance with the reported result [36-38]. In addition, the Fig. 5(a and d) also clearly demonstrate that the binding energies of Fe 2p_{3/2} are obtained at 714.5 eV and 714.3 eV, respectively, corresponding to the Fe³⁺-F bonds, consistent with previous reports [39,40]. The existence of FeF₃ is mainly ascribed to the side reaction of Fe₂O₃ and HF, and HF is formed as the consequence of hydrolysis of LiPF₆-based electrolyte [41,42].

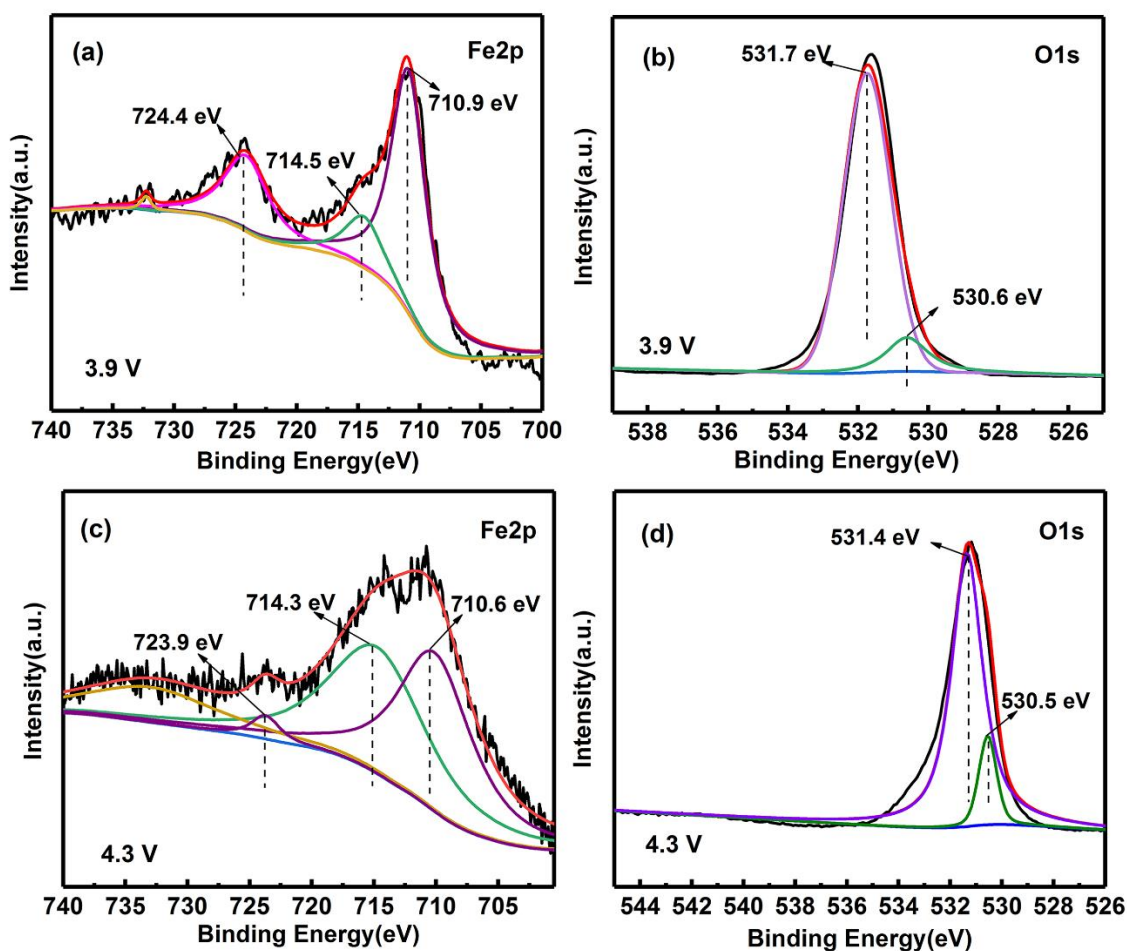


Figure 5. XPS spectra of the pristine Fe/Li₂O electrode surface at the different cut-off voltage states during the first constant current charging: (a) Fe 2p and (b) O 1s of 3.9 V, Fe 2p (c) and O 1s (d) of 4.3 V.

To better exhibit the initial electrochemical delithiation-lithiation process of the pristine Fe/Li₂O. The cyclic voltammogram (CV) curve of the pristine Fe/Li₂O for the first cycle at a scan rate of 0.1 mV s⁻¹ between 3.0 and 4.5 V (vs Li/Li⁺) at room temperature is shown in Fig. 6. Two distinct anodic peaks appear at around 3.86 V and 3.95 V during the delithiation process, respectively. The former broad peak is reasonably attributed to the electrochemical oxidation reaction transforming from Fe⁰ to Fe²⁺ and

further to Fe₃O₄ (Fe²⁺ and Fe³⁺) of intermediate valence, which is in accordance with the results of the binding energies of Fe 2p_{3/2} and Fe 2p_{1/2} appeared in the Fe 2p spectrum (Fig. 5(a)) and corresponds to the first two charge plateaus in Fig. 4(a). The second sharp peak stems from the thorough electrochemical oxidation reaction of Fe²⁺ or Fe₃O₄ (Fe²⁺ and Fe³⁺) to Fe³⁺, and corresponding to the third charge plateau in Fig. 4(a) and agreeing well with the result of the binding energies of Fe 2p_{3/2} and Fe 2p_{1/2} which are characterized by Fe³⁺ in the Fe 2p spectrum (Fig. 5(c)).

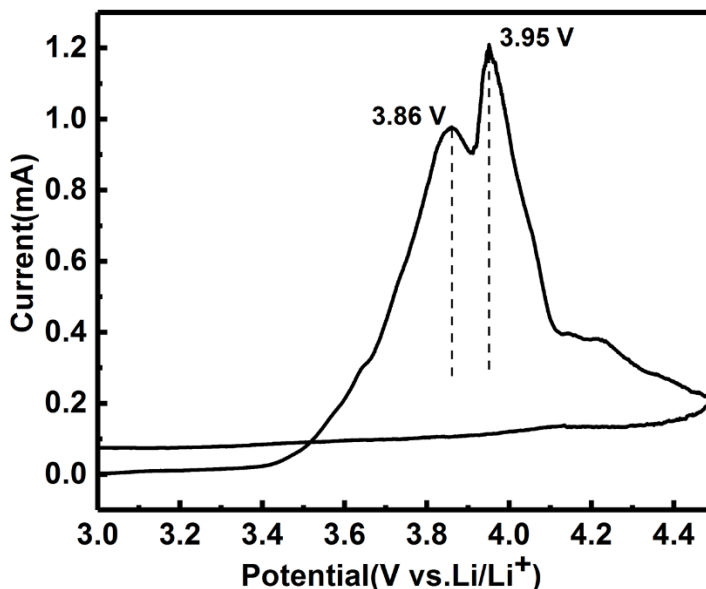
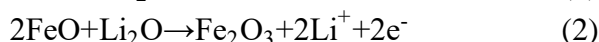


Figure 6. CV curve for the first cycle of the pristine Fe/Li₂O at a scan rate of 0.1 mV s⁻¹.

The delithiation process of the pristine Fe/Li₂O can be divided roughly into two steps as follows:



The electrochemical reaction mechanism of the pristine Fe/Li₂O can be expressed as $2\text{Fe} + 3\text{Li}_2\text{O} \rightarrow \text{Fe}_2\text{O}_3 + 6\text{Li}^+ + 6\text{e}^-$. In addition, there is no appearance of reduction peak in the CV curve, indicating that the Fe/Li₂O almost not participate in the embedded reaction of active lithium, and which further explains that the first discharge capacity of Fe/Li₂O is only reaching 6.9 mAh g⁻¹ (Fig. 4(a)). This means that Fe/Li₂O can be used as a cathode prelithiation additive in the voltage range of 3.0 V-4.5 V.

4. CONCLUSIONS

In this paper, Fe/Li₂O were successfully prepared by *in situ* solid phase reaction method. Fe/Li₂O can be used as a cathode prelithiation additive with a high prelithiation specific capacity of 447.3 mAh g⁻¹ during charging, and the first charge capacity of LiNi_{0.6}Co_{0.2}Mn_{0.2}O₂ with 7.5% Fe/Li₂O additive could be enhanced by 9.1% and its cycling stability was improved from 86.9% to 90.2% after 70 cycles. The cathode prelithiation additive could significantly increase the content of active lithium in the initial

delithiation process, contributing to form solid electrolyte interphase on the anode surface and better cycling stability.

Here we provide a simple, economical synthesis method to obtain the high-capacity cathode prelithiation additive for lithium ion batteries.

References

1. J.-M. Tarascon and M. Armand, *Nature*, 414 (2001) 359-367.
2. M. S. Whittingham, *Chem. Rev.*, 104 (2004) 4271-4301.
3. K. Kang, Y. S. Meng, J. Breger, C. P. Grey and G. Ceder, *Science*, 311(2006) 977-980.
4. M. Armand and J.-M. Tarascon, *Nature*, 451 (2008) 652-657 (2008).
5. J. B. Goodenough and K.-S. Park, *J. Am. Chem. Soc.*, 135 (2013) 1167-1176.
6. P. Verma, P. Maire and P. Novák, *Electrochim. Acta*, 55 (2010) 6332-6341.
7. K. Zaghib, G. Nadeau and K. Kinoshita, *J. Electrochem. Soc.*, 147 (2000) 2110-2115.
8. D. Aurbach, Y. Ein-Eli, B. Markovsky, A. Zaban, S. Luski, Y. Carmeli and H. Yamin, *J. Electrochem. Soc.*, 142 (1995) 2882-2890.
9. Y. Matsumura, S. Wang and J. Mondori, *J. Electrochem. Soc.*, 142 (1995) 2914-2918.
10. K. Xu, *Chem. Rev.*, 104 (2004) 4303-4417.
11. M. W. Forney, M. J. Ganter, J. W. Staub, R. D. Ridgley and B. J. Landi, *Nano Lett.*, 13 (2013) 4158-4163.
12. L. Ma, J. Self, M. Nie, S. Glazier, D. Y. Wang, Y.-S. Lin and J. R. Dahn, *J. Power Sources*, 299 (2015) 130-138.
13. J. Zhao, Z. Lu, N. Liu, H.-W. Lee, M. T. McDowell and Y. Cui, *Nat. Commun.*, 5 (2014) 5088.
14. J. Zhao, Z. Lu, H. Wang, W. Liu, H.-W. Lee, K. Yan, D. Zhuo, D. Lin, N. Liu and Y. Cui, *J. Am. Chem. Soc.*, 137 (2015) 8372-8375.
15. I. W. Seong, K. T. Kim and W. Y. Yoon, *J. Power Sources*, 189 (2009) 511-514.
16. Z. Wang, Y. Fu, Z. Zhang, S. Yuan, K. Amine, V. Battaglia and G. Liu, *J. Power Sources*, 260 (2014) 57-61.
17. K. Park, B.-C. Yu and J. B. Goodenough, *Adv. Energy Mater.*, 6 (2016) 1502534.
18. Y. Sun, Y. Li, J. Sun, Y. Li, A. Pei and Y. Cui, *Energy Storage Materials*, 6 (2017) 119-124.
19. M. Noh and J. Cho, *J. Electrochem. Soc.*, 159 (2012) A1329-A1334.
20. C. S. Johnson, S.-H. Kang, J. T. Vaughey, S. V. Pol, M. Balasubramanian and M. M. Thackeray, *Chem. Mater.*, 22 (2010) 1263-1270.
21. T. Okumura, M. Shikano and H. Kobayashi, *J. Mater. Chem. A*, 2 (2014) 11847-11856.
22. X. Su, C. Lin, X. Wang, V. A. Maroni, Y. Ren, C. S. Johnson and W. Lu, *J. Power Sources*, 324 (2016) 150-157.
23. L. Zhang, W. M. Dose, A. D. Vu and C. S. Johnson and W. Lu, *J. Power Sources*, 400 (2018) 549-555.
24. Y. Sun, H.-W. Lee, G. Zheng, Z. W. Seh, J. Sun, Y. Li and Y. Cui, *Nano Lett.*, 16 (2016) 1497-1501.
25. Y. Sun, H.-W. Lee, Z. W. Seh, N. Liu, J. Sun, Y. Li and Y. Cui, *Nat. Energy*, 1 (2016) 15008.
26. K. Rui, Z. Wen, Y. Lu, J. Jin and C. Shen, *Adv. Energy Mater.*, 5 (2015) 1401716.
27. X. Fan, Y. Zhu, C. Luo, T. Gao, L. Suo, S.-C. Liou, K. Xu and C. Wang, *J. Power Sources*, 307 (2016) 435-442.
28. S.-K. Jung, H. Gwon, J. Hong, K.-Y. Park, D.-H. Seo, H. Kim, J. Hyun, W. Yang and K. Kang, *Adv. Energy Mater.*, 4 (2014) 1300787.
29. M. Gu, I. Belharouak, J. Zheng, H. Wu, J. Xiao, A. Genc, K. Amine, S. Thevuthasan, D. R. Baer, J.-G. Zhang, N. D. Browning, J. Liu and C. Wang, *ACS Nano*, 7 (2013) 760-767.

30. N. Y. Kim, T. Yim, J. H. Song, J.-S. Yu and Z. Lee, *J. Power Sources*, 307 (2016) 641-648.
31. J. F. Anderson, M. Kuhn and U. Diebold, *Surf. Sci. Spectra*, 4 (1996) 266-272.
32. N. S. McIntyre and D. G. Zetaruk, *Anal. Chem.*, 49 (1977) 1521-1529.
33. J. Luo, J. Liu, Z. Zeng, C. F. Ng, L. Ma, H. Zhang, J. Lin, Z. Shen and H. J. Fan, *Nano Lett.*, 13 (2013) 6136-6143.
34. X. Hu, M. Ma, M. Zeng, Y. Sun, L. Chen, Y. Xue, T. Zhang, X. Ai, R. G. Mendes, M. H. Rummeli and L. Fu, *ACS Appl. Mater. Interfaces*, 6 (2014) 22527-22533.
35. J. Wang, H. Zhou, J. Nanda and P. V. Braun, *Chem. Mater.*, 27 (2015) 2803-2811.
36. D. Barreca, G. A. Battiston, D. Berto, R. Gerbasi and E. Tondello, *Surf. Sci. Spectra*, 8 (2001) 240-245.
37. J. F. Moulder, W. F. Stickle, P. E. Sobol and K. D. Bomben, *Handbook of X-ray photoelectron spectroscopy* (Ed: J. Chastain), Perkin-Elmer, Eden Prairie, MN 1992.
38. G. Bhargava, I. Gouzman, C. M. Chun, T. A. Ramanarayanan and S. L. Bernasek, *Appl. Surf. Sci.*, 253 (2007) 4322-4329.
39. A. P. Grosvenor, B. A. Kobe, M. C. Biesinger and N. S. McIntyre, *Surf. Interface Anal.*, 36 (2004) 1564-1574.
40. L. Li, V. Breedveld and D. W. Hess, *ACS Appl. Mater. Interfaces*, 4 (2012) 4549-4556.
41. D. Aurbach, A. Zaban, A. Schechter, Y. Ein-Eli, E. Zinigrad and B. Markovsky, *J. Electrochem. Soc.*, 142 (1995) 2873-2882.
42. S. J. An, J. Li, C. Daniel, D. Mohanty, S. Nagpure and D. L. Wood, *Carbon*, 105 (2016) 52-76.

© 2019 The Authors. Published by ESG (www.electrochemsci.org). This article is an open access article distributed under the terms and conditions of the Creative Commons Attribution license (<http://creativecommons.org/licenses/by/4.0/>).